Computed tomography with linear shift-invariant optical systems

Timur E. Gureyev,[1,*] Yakov I. Nesterets,[1] Konstantin M. Pavlov,[2] and Stephen W. Wilkins[1]

[1]*CSIRO Manufacturing and Materials Technology, PB33, Clayton Victoria 3169, Australia*
[2]*School of Physics, Monash University, Victoria 3800, Australia*
[*]*Corresponding author: Tim.Gureyev@csiro.au*

Received August 30, 2006; revised February 28, 2007; accepted March 17, 2007;
posted March 26, 2007 (Doc. ID 74579); published July 11, 2007

Optical systems capable of three-dimensional transmission imaging are considered; these systems employ a conventional tomographic setup with an added linear shift-invariant optical system between the sample and the detector. A theoretical analysis is presented of image formation and sample reconstruction in such systems, examples of which include diffraction tomography and phase-contrast tomography with the use of analyzer crystals. An example is introduced in which the image is obtained by scanning the beam along the line orthogonal to the optic axis and to the axis of rotation with a one-dimensional slit or grating parallel to the rotation axis. We show that under certain conditions the proposed system may allow quantitative local (region-of-interest) tomography. © 2007 Optical Society of America

OCIS codes: 110.6960, 340.7440, 100.5070, 100.6950.

1. INTRODUCTION

Computed tomography (CT) is a well-established technique for three-dimensional (3D) nondestructive imaging [1–3]. In its conventional form, CT is aimed at reconstructing the spatial distribution of the attenuation coefficient inside a sample from projection images collected at different orientations ("view angles") of the sample. In more recent times considerable effort has been directed toward the development of a theoretical basis and experimental means for diffraction and phase-contrast tomography [4–12]. The main motivation for that development was the desire to achieve higher contrast and signal-to-noise ratios in projection images (and ultimately, in the reconstructed 3D maps of the refractive index) of samples that do not display sufficient attenuation contrast. This is the case, for example, for different types of biological soft tissue, which often have similar x-ray attenuation properties leading to poor differentiation in conventional medical CT. Phase contrast is particularly useful when imaging samples that consist predominantly of low-Z elements using hard x rays (with energies of $\sim$10 keV and above). In this case the real part of the complex refractive index of the sample, which is responsible for the phase contrast, is typically several orders of magnitude larger than the imaginary part of the refractive index, which is responsible for absorption of x rays [7]. Unfortunately, the phase of x rays cannot be measured directly by conventional detectors owing to the very high frequency of the corresponding electromagnetic waves. Therefore it is necessary to convert the spatial variations of the phase in the transverse sections of the transmitted x-ray beam into detectable intensity variations (phase contrast). This conversion is usually performed by an optical system introduced between the sample and the detector. Different optical systems corresponding to different mechanisms of phase–amplitude conversion have been employed, including x-ray interferometers [7,8], x-ray lenses in the form of Fresnel zone plates [13] or compound refractive lenses [14], free-space propagation leading to in-line phase contrast [9–12], perfect analyzer crystals [15–17], and others. The process of extracting the phase distribution from collected phase-contrast images typically involves some form of computer processing of registered data. This computer processing can be relatively simple or quite sophisticated depending on the employed type of phase-contrast imaging. While the issue of numerical complexity of the phase retrieval algorithms is becoming less critical with the rapid progress in computer technology, the issue of noise sensitivity of the algorithms remains important. After the phase distribution in the transmitted wave is recovered, conventional methods for CT reconstruction can be applied to obtain the 3D distribution of the refractive index in the sample. Of the abovementioned techniques, the in-line method and the method using analyzer crystals can be readily associated with linear shift-invariant (LSI) optical systems located between the sample and the detector. In the present paper we extend this methodology (under certain assumptions about the sample properties) to generic LSI systems and also propose simple optical systems capable of producing detectable phase contrast.

One problem that is equally important in conventional and phase-contrast tomography is the nonlocality of the CT reconstruction [3,18,19]. "Nonlocality" here refers to the fact that a whole axial slice of the sample always has to be scanned and reconstructed even when one is only interested in the distribution of the refractive index in a small region of interest (ROI) within that slice. Mathematically, the nonlocality of the CT reconstruction can be traced to the nonlocality of the implicit Hilbert transform, although recently it was pointed out that the latter nonlocality may be less severe than was previously thought [20]. In a popular filtered backprojection method [3] the

nonlocality of CT reconstruction appears in the form of the Calderon operator (ramp filter). The latter operator has a convolution kernel whose Fourier transform is equal to $|\xi'|$, i.e., to the modulus of the independent variable in the Fourier space that corresponds to the direction orthogonal to the axis of rotation and to the optic axis. One of the questions considered in the present paper is that of the existence of physically realizable LSI systems with transfer functions proportional to $|\xi'|$. In other words we look for LSI systems that can perform appropriately filtered forward projection in hardware, thus eliminating the need for subsequent filtering of the backprojection in the CT reconstruction software. It is easy to show (see Section 2 below) that the CT reconstruction using projection images obtained with such an LSI system will result in a mutual cancellation of the ramp filter and the transfer function of the system, thus leading to a local reconstruction formula involving only the backprojection operation. This would appear to allow one to realize ROI tomography or to reconstruct objects that do not fit into the field of view of the imaging system. However, it is also clear that in general an LSI system with a transfer function proportional to $|\xi'|$ will itself be nonlocal (like most LSI systems). We show in the present paper that it may be possible to control the extent of this nonlocality by means of a suitable design of the optical system. If the extent of the nonlocality is much smaller than the dimensions of the ROI, then a form of local CT may still be possible. Note that as the ramp filter is responsible not only for the nonlocality of the CT reconstruction, but also for its mathematical instability [3], the implementation of this filter in hardware, instead of software, may in principle also increase the robustness of the CT reconstruction. Areas of potential practical applications of a system capable of local tomography are likely to include medical CT, inspection of microelectronic components at high spatial resolution, and many others.

2. COMPUTED TOMOGRAPHY WITH LINEAR SHIFT-INVARIANT OPTICAL SYSTEMS

Let a weakly absorbing object (sample) be illuminated by a plane monochromatic wave with wavelength λ and intensity I^{in}, and let the transmitted wave pass through some optical system before being registered by a position-sensitive detector (Fig. 1). We use Cartesian coordinates $\mathbf{r}=(x,y,z)$ to describe the spatial distribution of the refractive index in the sample, $n(\mathbf{r})\equiv 1-\Delta(\mathbf{r})+i\beta(\mathbf{r})$. The direction, z', of the incident wave, $\sqrt{I^{\text{in}}}\exp(ikz')$, where $k=2\pi/\lambda$, makes an angle θ' with the z axis, with $-\pi/2\le\theta'<\pi/2$. The complex amplitude of the transmitted wave in the plane $z'=0$ located immediately after the object can be written as $u_\theta^{\text{obj}}(x',y)=\sqrt{I^{\text{in}}}\exp[i\varphi_\theta(x',y)-\mu_\theta(x',y)]$, where $\mathbf{r}'=(x',y,z')$ are Cartesian coordinates rotated by angle θ' around the y axis with respect to coordinate system $\mathbf{r}$ and $\theta=\theta'+\pi/2$ (Fig. 1). We assume that the projection approximation can be applied to calculate the attenuation and the phase shift acquired by the wave upon transmission through the sample, i.e.,

$$\mu_\theta(x',y)=k(\mathbf{P}_\theta\beta)(x',y), \tag{1a}$$

$$\varphi_\theta(x',y)=-k(\mathbf{P}_\theta\Delta)(x',y), \tag{1b}$$

where $(\mathbf{P}_\theta f)(x',y)=\int_{-\infty}^{\infty}\int_{-\infty}^{\infty}f(x,y,z)\,\delta(x'-x\sin\theta-z\cos\theta)\,dx\,dz$ is the projection operator and $\delta(x)$ is the Dirac delta function.

We are interested in the reconstruction of the 3D distribution of the refractive index inside the sample, $n(\mathbf{r})$, using the information that can be extracted from the transmitted wave at different view angles θ. Taking the 2D Fourier transform, $(\mathbf{F}f)(\xi',\eta)=\int\int\exp[i2\pi(x'\xi'+y\eta)]f(x',y)\,dx'\,dy$, of Eqs. (1a) and (1b) and using the Fourier slice theorem, one can easily derive [3] that

$$\beta(x,y,z)=k^{-1}\int_0^{\pi}\int_{-\infty}^{\infty}\int_{-\infty}^{\infty}\exp\{-i2\pi[\xi'(x\sin\theta+z\cos\theta)+\eta y]\}(\mathbf{F}\mu_\theta)(\xi',\eta)|\xi'|\,d\xi'\,d\eta\,d\theta, \tag{2a}$$

$$\Delta(x,y,z)=-k^{-1}\int_0^{\pi}\int_{-\infty}^{\infty}\int_{-\infty}^{\infty}\exp\{-i2\pi[\xi'(x\sin\theta+z\cos\theta)+\eta y]\}(\mathbf{F}\varphi_\theta)(\xi',\eta)|\xi'|\,d\xi'\,d\eta\,d\theta. \tag{2b}$$

Therefore, if the projected values, $\mu_\theta(x',y)$ and $\varphi_\theta(x',y)$, can be obtained for all view angles θ in the interval $[0,\pi)$,

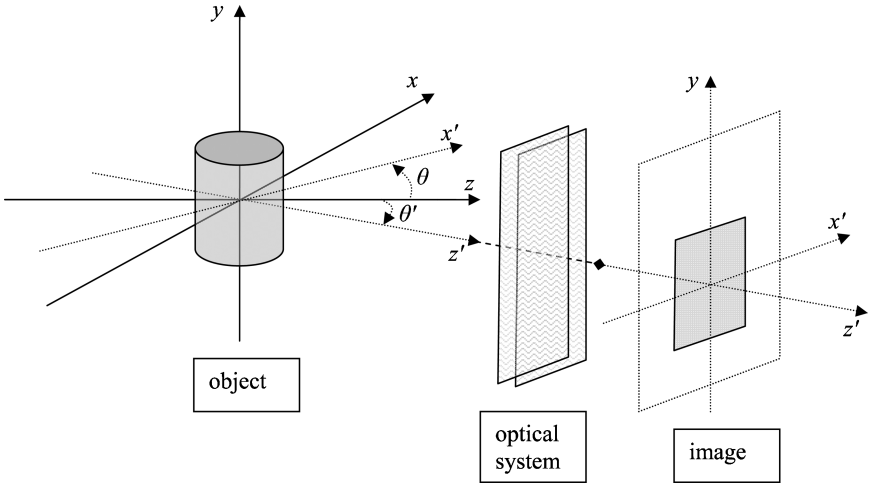

Fig. 1. Geometry of the CT setup with an added optical system.

Eqs. (2a) and (2b) can be used for the reconstruction of the 3D distribution of the complex refractive index. In conventional CT the values of $\mu_\theta(x',y)$ are obtained by measuring the 2D distribution of intensity in the object plane, $z'=0$, and evaluating $\mu_\theta(x',y)=0.5\ln[I^{\text{in}}/I^{\text{obj}}(x',y)]$. On the other hand, at x-ray frequencies it is difficult to measure the phase, $\varphi_\theta(x',y)$, of the transmitted electromagnetic wave directly. Therefore we consider a more practical approach to the reconstruction of the 3D distribution of the real part of the refractive index, using the measured distributions of intensity in the wave transmitted through the sample at different view angles after that wave has passed through some optical system that converted the phase variations in the transmitted wave in the object plane into detectable intensity variations in the detector plane (Fig. 1).

Let the propagation of a complex transmitted amplitude from the object plane to the detector plane be described by a LSI coherent optical system. Then the complex amplitude at the detector plane can be expressed as a convolution integral,

$$u_\theta^{\text{det}}(x',y)=\int\int u_\theta^{\text{obj}}(\tilde{x}',\tilde{y})G(x'-\tilde{x}',y-\tilde{y})\mathrm{d}\tilde{x}'\mathrm{d}\tilde{y}, \quad (3)$$

where $u_\theta^{\text{det}}(x',y)$ and $u_\theta^{\text{obj}}(x',y)$ are the complex amplitudes of the transmitted wave in the detector and object planes, respectively, and $G(x',y)$ is the point-spread function (PSF) of the optical system. We assume that the distribution of refractive index in the sample is such that at all view angles θ the attenuation is weak and the transmitted phase satisfies the Guigay-type condition [21], i.e.,

$$|\mu_\theta(x',y)|\ll 1, \quad (4a)$$

$$|\varphi_\theta(x',y)-\varphi_\theta(\tilde{x}',\tilde{y})|\ll 1, \quad (4b)$$

for all points (x',y) and $(\tilde{x}',\tilde{y})$ in the object plane that are separated by a distance smaller than the diameter of the essential support of the PSF G (the essential support of the function is understood as a region outside which the integral of the square modulus of that function is negligibly small). Condition (4b) means that the transmitted phase may consist of two components, one being small in magnitude, with the other changing slowly as a function of transverse coordinates [22]. It can be shown that the two components correspond to the first Born and the transport of intensity approximations, respectively [22]. Note that in the case of free-space propagation of the transmitted wave from the object to the detector (as in in-line phase tomography), when the support of $G^{\text{free}}(x',y)=i/(R\lambda)\exp[i\pi(x'^2+y^2)/(R\lambda)]\}$ is unbounded, condition (4b) can be relaxed to hold only for the points (x',y) and $(\tilde{x}',\tilde{y})$ separated by less than the distance $R\lambda/h_{\min}$, where $h_{\min}$ is the size of the smallest resolvable feature in the object [21,22].

Under conditions (4) we have

$$\exp[-\mu_\theta(x_1',y_1)-\mu_\theta(x_2',y_2)+i\varphi_\theta(x_1',y_1)-i\varphi_\theta(x_2',y_2)]$$
$$\cong 1-\mu_\theta(x_1',y_1)-\mu_\theta(x_2',y_2)+i\varphi_\theta(x_1',y_1)-i\varphi_\theta(x_2',y_2).$$

The last expression can be substituted into the equation for the detected intensity, $I_\theta^{\text{det}}(x',y)\equiv|u_\theta^{\text{det}}(x',y)|^2$, where the detector-plane amplitude is expressed by Eq. (3). Taking the Fourier transform of this intensity distribution, we arrive at the following expression:

$$\begin{aligned}(\mathbf{F}I_\theta^{\text{det}})(\xi',\eta)=I^{\text{in}}\{&|\mathbf{F}G|^2(0,0)\delta(\xi',\eta)-(\mathbf{F}\mu_\theta)(\xi',\eta)\\&\times[(\mathbf{F}G^*)(0,0)(\mathbf{F}G)(\xi',\eta)+(\mathbf{F}G)(0,0)\\&\times(\mathbf{F}G^*)(\xi',\eta)]+(\mathbf{F}\varphi_\theta)(\xi',\eta)[i(\mathbf{F}G^*)(0,0)\\&\times(\mathbf{F}G)(\xi',\eta)-i(\mathbf{F}G)(0,0)(\mathbf{F}G^*)(\xi',\eta)]\}.\end{aligned} \quad (5)$$

At this stage it is convenient to introduce the optical transfer function (OTF) $T(\xi',\eta)\equiv\mathbf{F}[G](\xi',\eta)$, the normalized OTF $\tilde{T}(\xi',\eta)\equiv T(\xi',\eta)/T(0,0)$, and the contrast function

$$K_\theta(x',y)\equiv 1-I_\theta^{\text{det}}(x',y)/[I^{\text{in}}|T(0,0)|^2]. \quad (6)$$

Then the following linear equation for the contrast function follows directly from Eqs. (5) and (6):

$$(\mathbf{F}K_\theta)(\xi',\eta)=2\tilde{T}^{\text{a}}(\xi',\eta)(\mathbf{F}\mu_\theta)(\xi',\eta)+2\tilde{T}^{\text{p}}(\xi',\eta)(\mathbf{F}\varphi_\theta)(\xi',\eta), \quad (7)$$

where the amplitude transfer function (ATF), $\tilde{T}^{\text{a}}(\xi',\eta)$, and the phase transfer function (PTF), $\tilde{T}^{\text{p}}(\xi',\eta)$, are defined in terms of the normalized OTF as follows (see also [23]):

$$\tilde{T}^{\text{a}}(\xi',\eta)=\frac{1}{2}\{\tilde{T}(\xi',\eta)+\tilde{T}^*(-\xi',-\eta)\},$$

$$\tilde{T}^{\text{p}}(\xi',\eta)=\frac{i}{2}\{-\tilde{T}(\xi',\eta)+\tilde{T}^*(-\xi',-\eta)\}.$$

Note that we have used the elementary general property of the Fourier transform, $\mathbf{F}[G^*](\xi',\eta)=\{(\mathbf{F}G)(-\xi',-\eta)\}^*$, to derive the last formulas. Both the ATF and the PTF are always Hermitian, e.g., $[\tilde{T}^{\text{a}}(\xi',\eta)]^*=\tilde{T}^{\text{a}}(-\xi',-\eta)$, and hence their inverse Fourier transforms, $\tilde{G}^{\text{a}}$ and $\tilde{G}^{\text{p}}$, are real functions that can be viewed as normalized amplitude and phase PSFs, respectively. If the normalized OTF, $\tilde{T}(\xi',\eta)$, is itself Hermitian, then the PTF vanishes, and hence such optical systems do not display phase contrast. A trivial example is the perfect imaging system, where $u_\theta^{\text{det}}(x',y)=u_\theta^{\text{obj}}(x',y)$, i.e., $G(x',y)=\delta(x',y)$. In this case $\tilde{T}^{\text{a}}(\xi',\eta)\equiv 1$ and $\tilde{T}^{\text{p}}(\xi',\eta)\equiv 0$. This case corresponds to conventional (amplitude) CT (considered here under the assumption of weak absorption).

Another immediate consequence of Eq. (7) is that within the accepted approximations [Eqs. (4)] a dark-field LSI optical system (i.e., a system with $T(0,0)=0$) does not produce any contrast (phase or amplitude), as in this case $(\mathbf{F}I_\theta^{\text{det}})(\xi',\eta)\equiv 0$ according to Eq. (5). A physical explanation of this phenomenon is that the (linear) contrast described by Eq. (7) is achieved as a result of interference of the direct and the weak scattered beam. In dark-field imaging systems the direct beam is absent by definition. Therefore the image intensity is negligibly small under the assumed conditions. Certainly, in reality the terms quadratic in phase and amplitude can contribute to the

image intensity in a dark-field imaging system, but these terms have been considered negligibly small under the accepted approximations.

If the intensity distribution in the detector plane, $I^{\mathrm{det}}_{\theta,j}(x',y)$, is measured at each view angle θ for two different states of the LSI system, $j=1,2$, then from Eq. (7) both the phase and the absorption distribution in the object plane can be recovered:

$$(\mathbf{F}\mu_\theta)(\xi',\eta) = \frac{\tilde{T}^{\mathrm{p}}_2(\xi',\eta)(\mathbf{F}K_{\theta,1})(\xi',\eta) - \tilde{T}^{\mathrm{p}}_1(\xi',\eta)(\mathbf{F}K_{\theta,2})(\xi',\eta)}{2[\tilde{T}^{\mathrm{a}}_1(\xi',\eta)\tilde{T}^{\mathrm{p}}_2(\xi',\eta) - \tilde{T}^{\mathrm{a}}_2(\xi',\eta)\tilde{T}^{\mathrm{p}}_1(\xi',\eta)]}, \quad (8a)$$

$$(\mathbf{F}\varphi_\theta)(\xi',\eta) = \frac{-\tilde{T}^{\mathrm{a}}_2(\xi',\eta)(\mathbf{F}K_{\theta,1})(\xi',\eta) + \tilde{T}^{\mathrm{a}}_1(\xi',\eta)(\mathbf{F}K_{\theta,2})(\xi',\eta)}{2[\tilde{T}^{\mathrm{a}}_1(\xi',\eta)\tilde{T}^{\mathrm{p}}_2(\xi',\eta) - \tilde{T}^{\mathrm{a}}_2(\xi',\eta)\tilde{T}^{\mathrm{p}}_1(\xi',\eta)]}, \quad (8b)$$

where the subscript indexes 1 and 2 used with the ATF, PTF, and contrast function correspond to the two states of the LSI system. If the denominator in Eqs. (8) is equal to zero at isolated points (ξ',η), then conventional Tichonov regularization can be applied to these equations. Substituting Eqs. (8) into Eqs. (2) we obtain general formulas for the reconstruction of the real and imaginary parts of the refractive index from the LSI CT data consisting of a pair of images for each view angle:

$$\beta(x,y,z) = \int_0^\pi \int_{-\infty}^{\infty}\int_{-\infty}^{\infty} \exp\{-i2\pi[\xi'(x\sin\theta + z\cos\theta) + \eta y]\} \times \frac{\tilde{T}^{\mathrm{p}}_2(\mathbf{F}K_{\theta,1}) - \tilde{T}^{\mathrm{p}}_1(\mathbf{F}K_{\theta,2})}{2k(\tilde{T}^{\mathrm{a}}_1\tilde{T}^{\mathrm{p}}_2 - \tilde{T}^{\mathrm{p}}_1\tilde{T}^{\mathrm{a}}_2)}(\xi',\eta)|\xi'|\mathrm{d}\xi'\mathrm{d}\eta\mathrm{d}\theta, \quad (9a)$$

$$\Delta(x,y,z) = \int_0^\pi \int_{-\infty}^{\infty}\int_{-\infty}^{\infty} \exp\{-i2\pi[\xi'(x\sin\theta + z\cos\theta) + \eta y]\} \times \frac{\tilde{T}^{\mathrm{a}}_2(\mathbf{F}K_{\theta,1}) - \tilde{T}^{\mathrm{a}}_1(\mathbf{F}K_{\theta,2})}{2k(\tilde{T}^{\mathrm{a}}_1\tilde{T}^{\mathrm{p}}_2 - \tilde{T}^{\mathrm{p}}_1\tilde{T}^{\mathrm{a}}_2)}(\xi',\eta)|\xi'|\mathrm{d}\xi'\mathrm{d}\eta\mathrm{d}\theta. \quad (9b)$$

In the case of free-space propagation between the object and the detector one has

$$\tilde{T}^{\mathrm{a}}_{\mathrm{TIE}}(\xi',\eta) = \cos[\pi\lambda R(\xi'^2+\eta^2)],$$

$$\tilde{T}^{\mathrm{p}}_{\mathrm{TIE}}(\xi',\eta) = -\sin[\pi\lambda R(\xi'^2+\eta^2)]. \quad (10)$$

Analogs of Eqs. (9) in this case (diffraction CT) were obtained previously [5]. Another example where Eqs. (9) have an immediate application is presented by the case of an LSI system consisting of a semiinfinite perfect crystal [24,25].

Now consider the case of phase CT. Here the sample is assumed to be nonabsorbing, i.e., $\beta(x,y,z)\equiv 0$. Then Eq. (7) gives a simple relationship between the distributions of measured contrast and the transmitted phase. Expressing $(\mathbf{F}\varphi_\theta)(\xi',\eta)$ from Eq. (7) with $\mu_\theta\equiv 0$ and substituting the result into Eq. (2b), we obtain

$$\Delta(x,y,z) = -\int_0^\pi \int_{-\infty}^{\infty}\int_{-\infty}^{\infty} \exp\{-i2\pi[\xi'(x\sin\theta + z\cos\theta) + \eta y]\} \frac{|\xi'|}{2k\tilde{T}^{\mathrm{p}}(\xi',\eta)}(\mathbf{F}K_\theta)(\xi',\eta)\mathrm{d}\xi'\mathrm{d}\eta\mathrm{d}\theta. \quad (11)$$

In the case of free-space propagation, the corresponding reconstruction formula for phase-contrast CT under the near-field condition, $h^2_{\min}/(R\lambda)\gg 1$ ($h_{\min}$ is the size of the smallest resolvable detail in the sample), was derived in [11]; in that case $\tilde{T}^{\mathrm{p}}_{\mathrm{TIE}}(\xi',\eta) = -\pi\lambda R(\xi'^2+\eta^2)$.

Note that if

$$\tilde{T}^{\mathrm{p}}(\xi',\eta) = p|\xi'|, \quad (12)$$

where p is a constant, then $|\xi'|$ in the numerator of Eq. (11) is cancelled out by the denominator, and the equation can be considerably simplified by evaluating the Fourier transform over (ξ',η), resulting in

$$\Delta(x,y,z) = (-2pk)^{-1}\int_0^\pi K_\theta(x\sin\theta + z\cos\theta, y)\mathrm{d}\theta. \quad (13)$$

According to Eq. (13), the reconstruction of the 3D distribution of the increment of the refractive index in the sample is accomplished by applying the backprojection operator to the 2D distributions of the contrast collected over the interval, $[0,\pi)$, of view angles θ. The usual filtering operation has disappeared owing to the special form of the PTF in Eq. (12). A similar reconstruction formula is applicable to a system with no phase contrast and $\tilde{T}^{\mathrm{a}}(\xi',\eta) = \tilde{p}|\xi'|$. Note, however, that an optical system is not allowed to have the OTF, $T(\xi',\eta)$, that is itself proportional to $|\xi'|$, as such an LSI system would be a dark-field one [as $T(0,\eta)\equiv 0$] and, hence, will not display any linear contrast as explained above.

The most important consequence of Eq. (13) is that in this case the CT reconstruction becomes local [3]; i.e., the value of the refractive index at an arbitrary point (x,y,z) inside the object is obtained from the x-ray projection values corresponding only to rays passing through the point (x,y,z) at all view angles θ. This property allows one to reconstruct regions of interest inside a sample that is larger than the field of view of the CT system. In the next section we analyze the question of the existence of physically realizable systems that might have a PTF or ATF of the type specified in Eq. (12) or that can be reduced to that type by applying simple and local image processing operations.

3. LSI WITH ONE-DIMENSIONAL SCANNING APERTURES

Consider an optical system consisting of a one-dimensional (1D) slit with width d located immediately before or immediately after an optically thin sample (Fig. 2). The Fourier transform of the distribution of transmitted intensity measured in the detector plane orthogonal to the optic axis z' at a distance R from the object plane $(z'=0)$ can be expressed as [21]

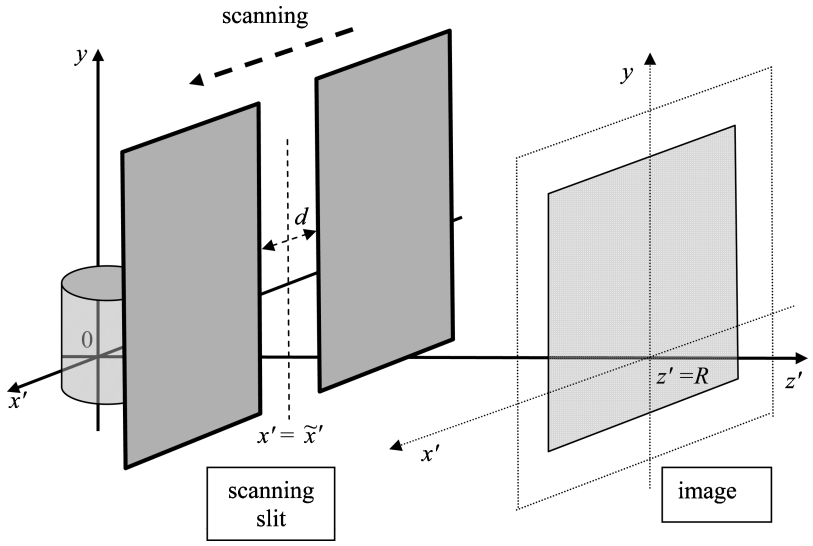

Fig. 2. Geometry of the CT setup with a scanning 1D slit.

$$(\mathbf{F}I_\theta^{\mathrm{det}})(\xi',\eta;R;\tilde{x}') = I^{\mathrm{in}}\int_{-\infty}^{+\infty}\int_{-\infty}^{+\infty}\exp(i2\pi[x'\xi'+y\eta])\times q_\theta(x'+\lambda R\xi'/2,y+\lambda R\eta/2)\times q_\theta^*(x'-\lambda R\xi'/2,y-\lambda R\eta/2)\times\chi_d(x'-\tilde{x}'+\lambda R\xi'/2)\times\chi_d^*(x'-\tilde{x}'-\lambda R\xi'/2)\mathrm{d}x'\mathrm{d}y, \quad (14)$$

where $q_\theta(x',y)=\exp[i\varphi_\theta(x')-\mu_\theta(x')]$ and $\chi_d(x')$ are the transmission functions of the object and the slit, respectively, and $\tilde{x}'$ is the coordinate of the position of the slit axis. We assume for simplicity that the transmission function $\chi_d(x')$ is equal to 1 when $|x'|<d/2$ and is equal to 0 otherwise, which corresponds to an ideal slit with rectangular edges. Integrating $(\mathbf{F}I_\theta^{\mathrm{det}})(\xi',\eta;R;\tilde{x}')$ over $\tilde{x}'$ (this corresponds to scanning the slit across the optical axis), we obtain a shift-invariant intensity distribution [26]:

$$(\mathbf{F}I_\theta^{\mathrm{SS}})(\xi',\eta;R) \equiv d^{-1}\int_{-\infty}^{+\infty}(\mathbf{F}I_\theta^{\mathrm{det}})(\xi',\eta;R;\tilde{x}')\mathrm{d}\tilde{x}' = (\mathbf{F}I_\theta^{\mathrm{PBI}})(\xi',\eta;R)\Lambda_\Xi(\xi'), \quad (15)$$

where $(\mathbf{F}I_\theta^{\mathrm{SS}})(\xi',\eta;R)$ and $(\mathbf{F}I_\theta^{\mathrm{PBI}})(\xi',\eta;R)$ are the Fourier transforms of the intensity distribution in the scanning slit image and that in the so-called propagation-based image (PBI) [$(\mathbf{F}I_\theta^{\mathrm{PBI}})(\xi',\eta;R)$ is described by Eq. (14) without the slit, i.e., with $\chi_d\equiv 1$], respectively, and $\Lambda_\Xi(\xi')$ is the modulation transfer function of the scanning slit:

$$\Lambda_\Xi(\xi') \equiv d^{-1}\int_{-\infty}^{+\infty}\chi_d(x')\chi_d(x'+\lambda R\xi')\mathrm{d}x' = \begin{cases}1-|\xi'|/\Xi & |\xi'|<\Xi\\ 0 & |\xi'|\geq\Xi\end{cases} \quad (16)$$

$\Xi\equiv d/(\lambda R)$. Note that the value of the cutoff spatial frequency, Ξ, can be easily adjusted by changing the width of the slit and/or the object-to-detector distance. The angular acceptance of the scanning system is limited to $(-\Xi,\Xi)$, which means that its spatial resolution is approximately limited by $1/\Xi=\lambda R/d$. Ideally, this spatial resolution should be finer then the size $h_{\min}$ of the minimal resolvable feature of the sample, i.e., $1/\Xi\leq h_{\min}$.

Defining a modified contrast function at each view angle as the normalized difference between the PBI image and the image obtained with the scanning slit system,

$$K_\theta^{\mathrm{SS}}(x',y;R) \equiv [I_\theta^{\mathrm{PBI}}(x',y;R) - I_\theta^{\mathrm{SS}}(x',y;R)]/I^{\mathrm{in}}, \quad (17)$$

we obtain that

$$(\mathbf{F}K_\theta^{\mathrm{SS}})(\xi',\eta;R) = [(\mathbf{F}I_\theta^{\mathrm{PBI}})(\xi',\eta;R)/I^{\mathrm{in}}]|\xi'|/\Xi, \quad \text{when } |\xi'|<\Xi. \quad (18)$$

Therefore the Fourier transform of this contrast function is proportional to the ramp filter, at least for suitably band-limited images.

Under the weak-object approximation, the following linearized expression for $(\mathbf{F}I_\theta^{\mathrm{PBI}})(\xi',\eta;R)$ can be derived from Eq. (14) with $\chi_d\equiv 1$ [21]:

$$(\mathbf{F}I_\theta^{\mathrm{PBI}})(\xi',\eta;R) = I^{\mathrm{in}}\{\delta(\xi',\eta) - 2\cos[\pi\lambda R(\xi'^2+\eta^2)]\times(\mathbf{F}\mu_\theta)(\xi',\eta) + 2\sin[\pi\lambda R(\xi'^2+\eta^2)]\times(\mathbf{F}\varphi_\theta)(\xi',\eta)\}. \quad (19)$$

Note that Eq. (19) can be obtained under less restrictive assumptions [22] than the weak-object approximation, Eqs. (4) used above.

It is useful to consider a class of samples with distributions of the real and imaginary parts of the refractive index that are proportional to each other, i.e., $\Delta(\mathbf{r})=\gamma\beta(\mathbf{r})$ (the proportionality constant γ does not depend on $\mathbf{r}$; nonabsorbing (phase) objects can be considered a limit case with $\gamma\to\infty$). Such proportionality can be easily shown to exist in the case of samples consisting of a single material [27] and also for objects consisting predominantly of light chemical elements ($Z<10$) in the case of x-rays with energies between approximately 60 and 500 keV [28]. For such samples $(\mathbf{F}\varphi_\theta)(\xi',\eta)=-\gamma(\mathbf{F}\mu_\theta)(\xi',\eta)$, and Eq. (19) for the PBI image intensity can be rewritten in terms of the

absorption coefficient alone. Also, in the case of near-field imaging, i.e., when $h_{\min}^2/(R\lambda) \gg 1$, the cosine function in Eq. (19) can be replaced by 1, and the sine function can be replaced by its argument [22]:

$$(\mathbf{F}I_\theta^{\mathrm{PBI}})(\xi',\eta;R) = I^{\mathrm{in}}\delta(\xi',\eta) - 2I^{\mathrm{in}}(\mathbf{F}\mu_\theta)(\xi',\eta) \times[1+\gamma\pi\lambda R(\xi'^2+\eta^2)]. \quad (20)$$

Combining Eq. (20) with Eq. (18) and using the fact that $\delta(\xi')|\xi'| = 0$, we find that in this case the Fourier transform of the contrast function is equal to

$$(\mathbf{F}K_\theta^{\mathrm{SS}})(\xi',\eta;R) = 2(\mathbf{F}\mu_\theta)(\xi',\eta)[1+\gamma\pi\lambda R(\xi'^2+\eta^2)] \times|\xi'|/\Xi, \quad |\xi'| < \Xi. \quad (21)$$

Expressing $(\mathbf{F}\mu_\theta)(\xi',\eta)$ from Eq. (21) and substituting the result into Eq. (2a), we obtain

$$\beta(x,y,z) = \frac{d}{4\pi R}\int_0^\pi \int_{-\infty}^{\infty}\int_{-\infty}^{\infty} \exp\{-i2\pi[\xi'(x\sin\theta + z\cos\theta) + \eta y]\} \times \frac{\mathbf{F}K_\theta^{\mathrm{SS}}(\xi',\eta;R)}{1+\gamma\pi\lambda R(\xi'^2+\eta^2)}\mathrm{d}\xi'\mathrm{d}\eta\mathrm{d}\theta, \quad (22)$$

where we replaced Ξ by $d/(\lambda R)$ in accordance with the definition of Ξ. Applying the differential operator $1-[\gamma\lambda R/(4\pi)]\nabla^2$, $\nabla^2 \equiv \partial_x^2+\partial_y^2+\partial_z^2$, to both sides of Eq. (22), we find

$$(R/d)(4\pi - \gamma\lambda R\nabla^2)\beta(x,y,z) = \int_0^\pi \int_{-\infty}^{\infty}\int_{-\infty}^{\infty} \exp\{-i2\pi[\xi'(x\sin\theta + z\cos\theta) + \eta y]\} \times(\mathbf{F}K_\theta^{\mathrm{SS}})(\xi',\eta;R)\mathrm{d}\xi'\mathrm{d}\eta\mathrm{d}\theta. \quad (23)$$

Finally, evaluating the Fourier transform over (ξ',η) in Eq. (23), we obtain

$$(R/d)(4\pi - \gamma\lambda R\nabla^2)\beta(x,y,z) = \int_0^\pi K_\theta^{\mathrm{SS}}(x\sin\theta + z\cos\theta, y; R)\mathrm{d}\theta. \quad (24)$$

Equation (24) shows that under the above conditions the 3D distribution of the result of application of a second-order elliptical differential operator (which is, therefore, local), $(R/d)(4\pi-\gamma\lambda R\nabla^2)$, to the imaginary part of the refractive index can be reconstructed in a local manner from the contrast function $K_\theta^{\mathrm{SS}}(x',y;R)$. Let $\chi_1^A(x')$ be the characteristic function of the interval $[-A,A]$, i.e., $\chi_1^A(x') \equiv 1$ when $|x'| \le A$ and $\chi_1^A(x') \equiv 0$ when $|x'| > A$; and let $\chi_2^A(x,z)$ be the characteristic function of the disk (ROI) $x^2+z^2 \le A^2$, i.e., $\chi_2^A(x,z) \equiv 1$ when $x^2+z^2 \le A^2$ and $\chi_2^A(x,z) \equiv 0$ when $x^2+z^2 > A^2$. The locality of Eq. (24) implies that

$$(R/d)\chi_2^A(x,z)(4\pi - \gamma\lambda R\nabla^2)\beta(x,y,z) = \chi_2^A(x,z)\int_0^\pi \chi_1^A(x\sin\theta + z\cos\theta) \times K_\theta^{\mathrm{SS}}(x\sin\theta + z\cos\theta, y; R)d\theta, \quad (25)$$

i.e., for any fixed y, the distribution of the function $(4\pi/\gamma\lambda R - \nabla^2)\beta(x,y,z)$ inside the disk $x^2+z^2 \le A^2$ can be reconstructed from projections $I_\theta^{\mathrm{PBI}}(x',y;R)$ and $I_\theta^{\mathrm{SS}}(x',y;R)$ [used in the definition of the contrast function $K_\theta^{\mathrm{SS}}(x',y;R)$] truncated (apertured) to the interval $|x'| \le A$.

The local reconstruction described by Eq. (25) corresponds to the experimental arrangement where the detector is smaller than the field of view (the size of the projection of the object). This can be also formally described by the presence of an aperture function $\chi_1^A(x')$ immediately in front of the detector. Another relevant experimental arrangement corresponds to the situation where the extent of the incident beam along the x' direction is smaller than the extent of the object along that direction. Within the formalism considered above this arrangement can be described by an aperture function $\tilde{\chi}_1^{A'}(x')$ located immediately before or immediately after the object, where $\tilde{\chi}_1^{A'}(x')$ is equal to 1 when $|x'| \le A'$ $(A' > A)$, is 0 when $|x'| > A' + a'$, and changes monotonically and smoothly from 1 to zero in the intervals $A' < |x'| < A' + a'$. In this case the Fourier transform of the projected absorption distribution in Eqs. (20) and (21) is replaced by $\mathbf{F}[\tilde{\chi}_1^{A'}(x')\mu_\theta(x',y)]$. The size a' of the smooth transition region should be chosen sufficiently large for Eq. (20) to be valid with the function $\tilde{\chi}_1^{A'}(x')\mu_\theta(x',y)$ in place of $\mu_\theta(x',y)$ (see the details in Appendix A).

In an experiment, it will be desirable to use apertures with rounded or wedgelike edges to reduce x-ray diffraction at the edges, but it may be difficult to eliminate the diffraction completely. Note, however, that as the detector plane is located within the near-field region with respect to the object, the spread of the diffraction fringes from the geometric images of aperture edges will be limited to the larger of the width of the first Fresnel zone, $(R\lambda)^{1/2}$, and that of the PSF of the imaging system. Note also that intensity value, $I_\theta^{\mathrm{SS}}(x',y;R)$, at a point (x',y,R) (and as a consequence, the value of the contrast function $K_\theta^{\mathrm{SS}}(x',y;R) \equiv [I_\theta^{\mathrm{PBI}}(x',y;R) - I_\theta^{\mathrm{SS}}(x',y;R)]/I^{\mathrm{in}}$ at that point) depends on the projection values, $(\mathbf{P}_\theta\beta)(x',y;\theta)$, within some vicinity $(x'-a, x'+a)$ of x'. Assuming that the width of the region of interest is much larger than the slit size, the value of a can be obtained from Eq. (15) as the width of the function $(\mathbf{F}^{-1}\Lambda_\Xi)(x') = \sin^2(\pi\Xi x')/(\pi^2\Xi x'^2)$, i.e., $a \sim 1/\Xi = R\lambda/d$. This means that in order to reconstruct the distribution of the refraction index within a given region of interest Ω inside the object, one will have to irradiate and scan a larger region Ω_a. This is a manifestation of the fact that the scanning slit system is itself nonlocal. The locality seemingly improves (i.e., $\Omega_a \to \Omega$) when $\Xi \to \infty$. Unfortunately, in the scanning-slit system there is a trade-off between the locality and the contrast. Indeed, the contrast diminishes when $\Xi \to \infty$, as can be

seen immediately from Eqs. (18). These issues are considered in more detail in Appendix A.

If the ROI is surrounded by an area with constant refraction and absorption properties, then the periodic or other uniform boundary conditions can be imposed on the distribution of β at the boundary of the region, and the operator in the left-hand side of Eq. (24) can be easily inverted [27] producing a 3D distribution of the imaginary part, $\beta(\mathbf{r})$, of the complex refractive index inside the ROI:

$$\beta(x,y,z) = (d/R)(4\pi - \gamma\lambda R\nabla^2)^{-1} \times \int_0^{\pi} K_\theta^{\mathrm{SS}}(x\sin\theta + z\cos\theta, y; R)\mathrm{d}\theta. \quad (26)$$

Note that in this case we can also reconstruct the real part of the refractive index according to $\Delta(\mathbf{r}) = \gamma\beta(\mathbf{r})$.

A local reconstruction formula for the case of a pure phase object ($\beta \equiv 0$) can be derived in a manner similar to Eq. (24); the result can be formally obtained by discarding the 4π term in the brackets on the left-hand side of Eq. (24) and noting that $\Delta(\mathbf{r}) = \gamma\beta(\mathbf{r})$. The pure phase case corresponds to $\gamma \to \infty$ or, more precisely, $2N_F \ll \gamma$, where $N_F = h_{\min}^2 k/R$ and $h_{\min}$ is the size of the smallest resolvable detail in the object as defined above. At the other limit, when $2N_F \gg \gamma$, we have the case of conventional CT, where the first term in brackets on the left-hand side of Eq. (24) is much larger than the second term. This corresponds to the case where the diffraction terms in Eq. (19) are negligibly small. Such a case can be realized, e.g., by choosing a sufficiently short sample-to-detector distance R. At the same time, the value of the cutoff frequency, Ξ, can be kept constant, if we decrease the slit width, d, accordingly. Therefore, in this case we end up with an analog of Eq. (24) without the Laplacian on the left-hand side, which represents a local CT reconstruction formula for absorption CT:

$$(4\pi R/d)\beta(x,y,z) \approx \int_0^{\pi} K_\theta^{\mathrm{SS}}(x\sin\theta + z\cos\theta, y; R)\mathrm{d}\theta. \quad (27)$$

The same equation can be obtained for the CT reconstruction with a scanning-slit system where the propagation distance R is optimized with respect to the x-ray source size and detector resolution in accordance with the recently proposed deblur by defocus method [22,29] even when absorption is not weak.

We briefly consider one simple but potentially important extension of the data acquisition strategy suggested above with the use of a scanning slit. One possible disadvantage of the latter system is the amount of time that may be required to scan the slit across the incident or transmitted beam at each angle of view. This exposure time can be substantially reduced if a single slit with transmission function $\chi_d(x')$ is replaced by a 1D periodic grating with transmission function $X_d(x') = \sum_{m=-M}^{M} \chi_d(x' + 2dm)$. Provided that M is sufficiently large (in practice Md should be slightly larger than the projection of the ROI onto the object plane), the transmission function $X_d(x')$ is effectively periodic in x' with period $2d$. Then in order to achieve the desired shift invariance of the scanned image it is sufficient to integrate the corresponding transmitted intensity over a single period:

$$(\mathbf{F}I_\theta^{\mathrm{SG}})(\xi', \eta; R) \equiv d^{-1}\int_{-d}^{+d} (\mathbf{F}\tilde{I}_\theta^{\mathrm{det}})(\xi', \eta; R; \tilde{x}')\mathrm{d}\tilde{x}' = (\mathbf{F}I_\theta^{\mathrm{PBI}})(\xi', \eta; R)\sum_{m=-M}^{M} \Lambda_\Xi(\xi' + 2m\Xi), \quad (28)$$

where $(\mathbf{F}I_\theta^{\mathrm{SG}})(\xi', \eta; R)$ is the Fourier transform of the intensity distribution in the scanning grating image and $(\mathbf{F}\tilde{I}_\theta^{\mathrm{det}})(\xi', \eta; R; \tilde{x}')$ is the image intensity corresponding to a fixed position of the grating [it is described by Eq. (14) with the function $X_d(x')$ in place of $\chi_d(x')$]. If, as above, the spatial Fourier spectrum of the PBI is limited to the interval $(-\Xi, \Xi)$, then the sum in Eq. (28) can be replaced by the single term corresponding to $m = 0$. This makes Eq. (28) identical to Eq. (15), which was obtained for a single scanning slit, with one important difference, i.e., we only have to translate the grating within a single period to obtain Eq. (28). This difference in the scanning requirements can be very significant for reducing the overall time of the CT data acquisition.

4. NUMERICAL SIMULATIONS

We have performed numerical simulations in order to verify the theoretical results obtained in the previous section. We simulated a phantom object consisting of five cylinders (Fig. 3): 1, a nylon cylinder of diameter 1000 μm; 2, a Kevlar cylinder of diameter 100 μm; 3 and 4, two cylinders of diameter 300 μm filled with olive oil; and, 5, a cylinder of diameter 400 μm also filled with olive oil. The density, chemical composition, and x-ray refractive index for the constituent materials are presented in Table 1. All the materials have similar values of $\gamma \equiv \Delta/\beta$ at the chosen energy $E = 25$ keV; i.e., the object approximately satisfies the homogeneous model $\Delta(\mathbf{r}) = \gamma\beta(\mathbf{r})$ used in Section 4 above. The positions of the cylinders in polar coordinates (ρ, φ) centered at the axis of cylinder 1 were, 1, $\rho = 0$, $\varphi = 0$; 2, $\rho = 40$ μm, $\varphi = \pi$; 3, $\rho = 280$ μm, $\varphi = 1.99$ rad; 4, $\rho = 280$ μm, $\varphi = 2.19$ rad; and, 5, $\rho = 260$ μm, $\varphi = 0$.

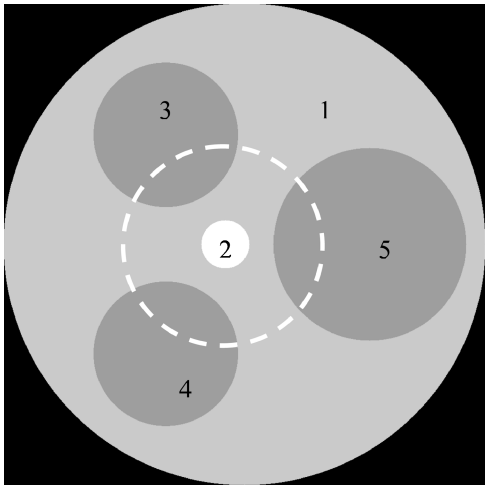

Fig. 3. Distribution of the real part of the refractive index decrement in the phantom.

Table 1. Chemical Composition, Density and X-Ray Refractive Indexes (at $E=25$ keV) for Materials Used in the Simulated Phantom

Material	Chemical Formula	Density, g/cm^3	μ/ρ, cm^2/g	μ, cm^{-1}	Δ	β	$\Delta\varphi$, rad/mm	Δ/β
1. Nylon	$C_{12}H_{22}N_2O_2$	1.14	0.313	0.357	0.4148×10^{-6}	1.4089×10^{-10}	−52.55	2944
2. Kevlar	$C_{14}H_{10}N_2O_2$	1.44	0.306	0.441	0.4977×10^{-6}	1.7404×10^{-10}	−63.06	2860
3–5. Olive oil	$C_{57}O_6H_{113}$ (approx.)	0.92	0.3	0.276	0.3436×10^{-6}	1.0892×10^{-10}	−43.53	3155

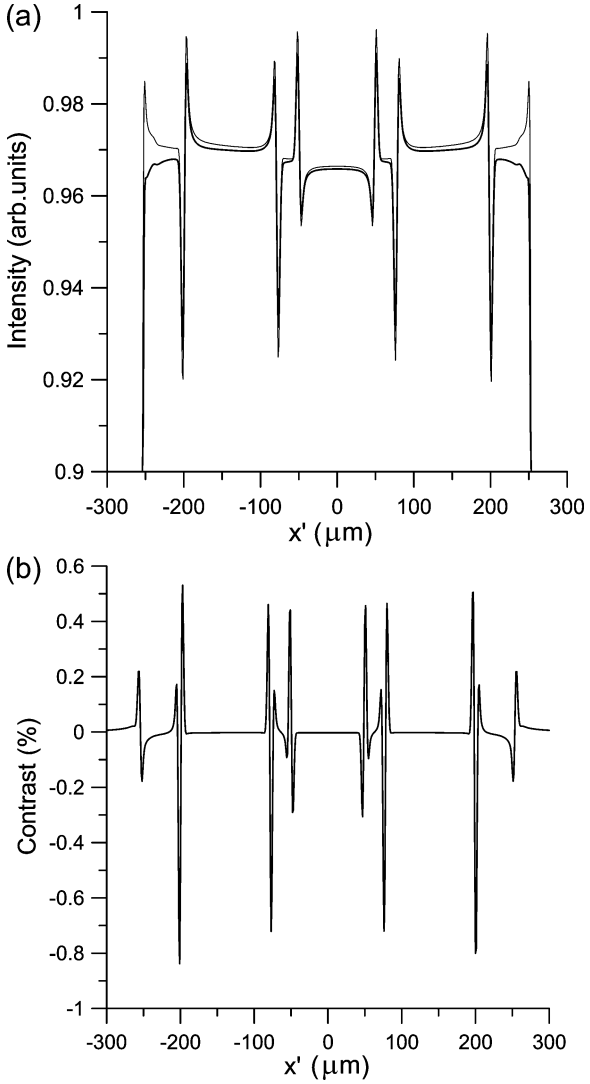

Fig. 4. (a) Example of calculated intensity distributions $I_\theta^{SG}(x';R)$ (thick curve) and $I_\theta^{PBI}(x';R)$ (thin curve); (b) Corresponding contrast function $K_\theta^{SG}(x';R)$ at the same view angle as in (a).

We then simulated CT projection data for the phantom. The irradiation of the sample was limited to a vicinity of cylinder 2, which was chosen as the ROI. The selected vicinity of the ROI is shown by a dashed circle in Fig. 3. The center of the tomographic rotation was set at 100 μm to the left from the axis of cylinder 1. We calculated 721 tomographic scans in the interval $[0,\pi]$. Each calculated projected intensity distribution contained 1024 pixels of size 1 μm. We also modeled the effect of detector resolution by convolving the projected intensity profiles with a

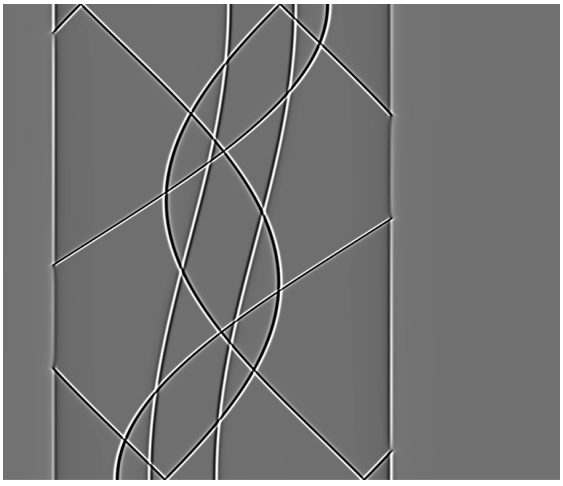

Fig. 5. Contrast sinogram of the vicinity of the ROI in the phantom obtained with a scanning 1D grating.

Gaussian distribution with standard deviation $\sigma=2$ μm representing the PSF of the detector. We calculated projected intensity distributions $I_\theta^{SG}(x';R)$ and $I_\theta^{PBI}(x';R)$, with and without the scanning 1D grating, at the sample-to-detector distance $R=20$ cm at each of the 721 rotation angles. Examples of these intensity distributions are shown in Fig. 4(a). The grating had a period of 10 μm with the equal sizes of transparent and opaque regions ($d=5$ μm). The contrast function, $K_\theta^{SG}(x';R)\equiv[I_\theta^{PBI}(x';R)-I_\theta^{SG}(x';R)]/I^{in}$, was calculated at each view angle. Figure 4(b) shows an example of the contrast function at a fixed view angle, while Fig. 5 contains the complete sinogram, i.e., the gray-scale representation of the contrast as a function of the view angle. Application of the backprojection operator to the contrast function, $K_\theta^{SG}(x';R)$, produced the result shown in Fig. 6(a). The dashed square in Fig. 6(a) delineates a subregion including cylinder 2. As the part of the phantom contained in the subregion can be viewed as a homogeneous object inside a uniform medium [30], one can use Eq. (24) for its quantitative description, with contrast function $K_\theta^{SG}(x';R)$ in place of $K_\theta^{SS}(x';R)$ and the values of β and Δ equal to the difference of the corresponding values for cylinders 1 and 2 (see Table 1). Equation (24) can be easily solved within the selected subregion to obtain the distribution of $\Delta\beta\equiv\beta_2-\beta_1$ in the vicinity of cylinder 2 [Fig. 6(b)]. One can see that the shape of the cylinder is reproduced quite accurately with the slight blurring of the edges caused by the finite spatial resolution of the imaging system. In Fig. 7 we present a cross section along the dashed square shown in Fig. 6(b), i.e., a cross section of the reconstructed distribution

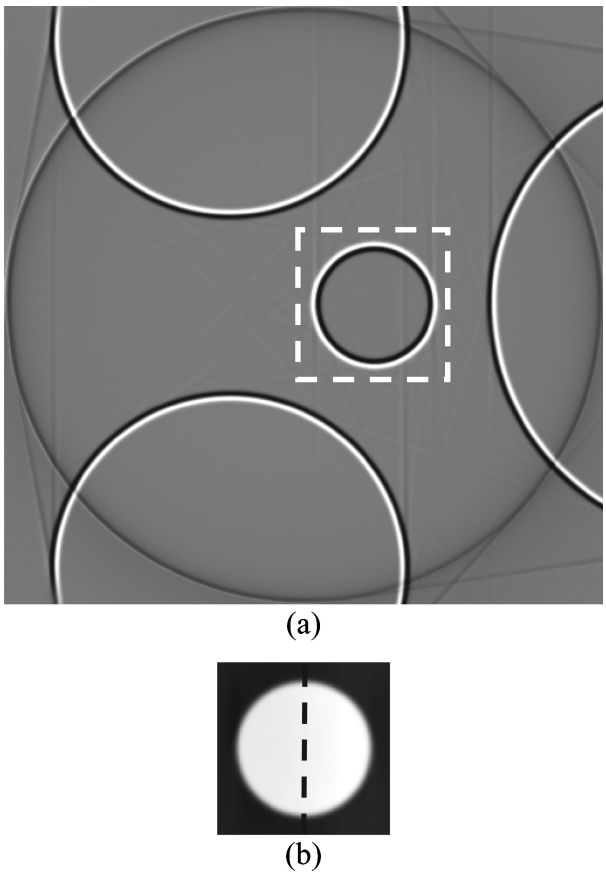

Fig. 6. (a) Backprojection of the contrast sinogram of Fig. 5; (b) the result of application of the operator $(R/d)(4\pi-\gamma\lambda R\nabla^2)^{-1}$ to the central part of (a).

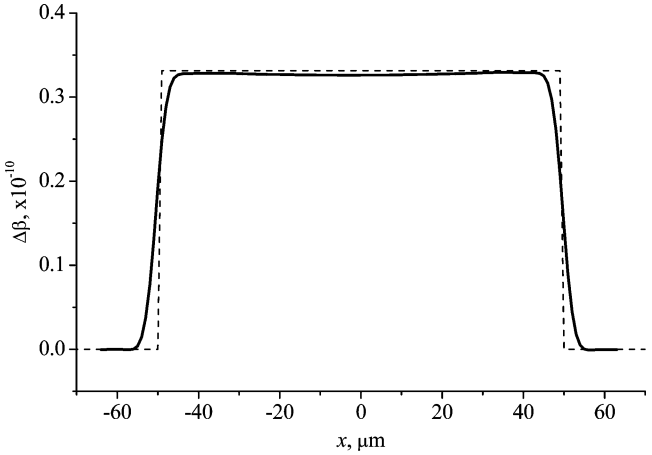

Fig. 7. Vertical cross-section along the dashed square in Fig. 6(b), showing the reconstructed distribution of the real part of the refractive index in the ROI.

of the imaginary part of refractive index inside the ROI. Obviously, the original distribution of the refractive index in cylinder 2 has been reconstructed with good accuracy.

5. CONCLUSIONS

We have analyzed the theory of image formation and sample reconstruction in CT with an LSI system inserted between the sample and the detector. The analysis has been performed by using a generalized weak-object model for the sample. We showed that under this approximation the detected 2D intensity distribution at each view angle represents a difference between the incident intensity and a weighted sum of the projected values of the spatial distribution of the real and imaginary parts of the refractive index in the sample, with the weights identified as the phase and amplitude transfer functions (PTF and ATF), respectively. Combining this result with the conventional formula for the inverse Radon transform, we demonstrated that when the ATF or PTF of the LSI system are proportional to $|\xi'|$, i.e., to the modulus of the appropriate independent variable in the Fourier space, the inverse Radon transform may be reduced to the backprojection operator.

We then proposed and analyzed an optical system consisting of a 1D slit or grating that is scanned along the line orthogonal to the axis of sample rotation and to the optic axis. Integrating the transmitted intensity with respect to the position of the slit or grating produces an image that can be shown to correspond to an LSI optical system with the ATF and PTF proportional to the Lambda function, $\Lambda_\Xi(\xi')=\max\{0,(1-|\xi'|/\Xi)\}$. Subtracting this image from an in-line image collected without the slit results in a contrast distribution that corresponds to a transfer function proportional to $|\xi'|$ within the interval $|\xi'|<\Xi$, where the value of cutoff frequency Ξ is determined by the x-ray wavelength, sample-to-detector distance, and width of the slit. If $1/\Xi$ is smaller than the size of the smallest resolvable feature in the in-line projection images, then this system performs the required 1D angular filtering of the forward projection in hardware, thus eliminating the need for software ramp filtering. As the latter filtering is the source of the nonlocality in conventional CT, its elimination results in a local reconstruction formula. The approximate locality of this CT system means that it is sufficient to collect x-ray intensity values corresponding only to the rays passing through a vicinity of the ROI inside the sample at each view angle, in order to reconstruct the 3D spatial distribution of the real or imaginary part (depending on the implementation) of the refractive index in that region. We have also verified the validity of the proposed image acquisition and sample reconstruction schemes by suitable numerical simulations.

APPENDIX A

Let us consider the case where the 1D beam-blocking aperture $\tilde{\chi}_1^{A'}(x')$ is located in the object plane. We assume that the aperture function $\tilde{\chi}_1^{A'}(x')\equiv 1$ for all $x'\in[A',A']$, and that $\tilde{\chi}_1^{A'}(x')$ smoothly and monotonically changes from 1 to 0 outside this interval. We determine the properties of the function $\tilde{\chi}_1^{A'}(x')$ required for the contrast $K_\theta^{SS}(x',y;R;A')\equiv[I_\theta^{PBI}(x',y;R;A')-I_\theta^{SS}(x',y;R;A')]/I^{in}$, obtained with this aperture, to coincide with the contrast $K_\theta^{SS}(x',y;R)\equiv[I_\theta^{PBI}(x',y;R)-I_\theta^{SS}(x'y;R)]/I^{in}$, obtained without the aperture, at least within a smaller interval $x'\in[-A,A]$.

The PBI amplitude and intensity distributions can be expressed as follows (as the second transverse coordinate, y, is irrelevant for the calculations presented below, we omit it in order to simplify the notation):

$$u_\theta^{\mathrm{PBI}}(x';R;A') = u^{\mathrm{in}}\int_{-\infty}^{+\infty}\exp(-i2\pi x'\xi')\times\exp(-i\pi\lambda R\xi'^2)(\mathbf{F}Q_\theta)(\xi')\mathrm{d}\xi',$$

$$(\mathbf{F}I_\theta^{\mathrm{PBI}})(\xi';R;A') = I^{\mathrm{in}}\int_{-\infty}^{+\infty}\exp[i2\pi\lambda R\xi'\zeta](\mathbf{F}Q_\theta)(\zeta+\xi'/2)\times(\mathbf{F}Q_\theta)^*(\zeta-\xi'/2)\mathrm{d}\zeta$$

$$= I^{\mathrm{in}}\int_{-\infty}^{+\infty}\exp(i2\pi x'\xi')Q_\theta(x'+\lambda R\xi'/2)\times Q_\theta^*(x'-\lambda R\xi'/2)\mathrm{d}x', \quad \text{(A1)}$$

where $Q_\theta(x')=\tilde{q}_\theta(x')\chi_{A'}(x')$ with $\chi_{A'}(x')=|\tilde{\chi}_1^{A'}(x')|$ and $\tilde{q}_\theta(x')=\exp[-\mu_\theta(x')+i\tilde{\varphi}_\theta(x')]$ with $\tilde{\varphi}_\theta(x')=\varphi_\theta(x')+\arg\tilde{\chi}_1^{A'}(x)$.

Equation (A1) can be written in an equivalent form:

$$(\mathbf{F}I_\theta^{\mathrm{PBI}})(\xi';R;A')/I^{\mathrm{in}} = (\mathbf{F}I_{\mathrm{FF}}^{\mathrm{PBI}})(\xi';R;A') - \int_{-\infty}^{+\infty}\exp(i2\pi x'\xi')\times[M_\theta(x'+\lambda R\xi'/2)\chi_{A'}^*(x'-\lambda R\xi'/2) + M_\theta^*(x'-\lambda R\xi'/2)\chi_{A'}(x'+\lambda R\xi'/2)]\mathrm{d}x' + i\int_{-\infty}^{+\infty}\exp(i2\pi x'\xi')[\Phi_\theta(x'+\lambda R\xi'/2)\times\chi_{A'}^*(x'-\lambda R\xi'/2) - \Phi_\theta^*(x'-\lambda R\xi'/2)\times\chi_{A'}(x'+\lambda R\xi'/2)]\mathrm{d}x', \quad \text{(A2)}$$

where

$$(\mathbf{F}I_{\mathrm{FF}}^{\mathrm{PBI}})(\xi';R;A') \equiv \int_{-\infty}^{+\infty}\exp(i2\pi x'\xi')\chi_{A'}(x'+\lambda R\xi'/2)\chi_{A'}^*(x'-\lambda R\xi'/2)\mathrm{d}x'$$

is the flat field (intensity distribution in the absence of the object), $M_\theta(x')\equiv\mu_\theta(x')\chi_{A'}(x')$, and $\Phi_\theta(x')\equiv\tilde{\varphi}_\theta(x')\chi_{A'}(x')$.

Consider separately the following function:

$$F(\xi') = \int_{-\infty}^{+\infty}\exp(i2\pi x'\xi')M_\theta(x'+\lambda R\xi'/2)\times\chi_{A'}^*(x'-\lambda R\xi'/2)\mathrm{d}x' = \exp(-i\pi\lambda R\xi'^2)\int_{-\infty}^{+\infty}\exp[-i2\pi\lambda R\xi'\zeta](\mathbf{F}M_\theta)(\zeta+\xi')\times(\mathbf{F}\chi_{A'})^*(\zeta)\mathrm{d}\zeta. \quad \text{(A3)}$$

Using the Taylor expansion of the function $(\mathbf{F}M_\theta)(\zeta+\xi')$,

$$(\mathbf{F}M_\theta)(\zeta+\xi') = \sum_{n=0}^{\infty}\frac{\zeta^n}{n!}(\mathbf{F}M_\theta)^{(n)}(\xi'),$$

we obtain the following result for the function $F(\xi')$,

$$F(\xi') = \exp(i\pi\lambda R\xi'^2)\sum_{n=0}^{\infty}\frac{1}{n!\,(2\pi i)^n}(\mathbf{F}M_\theta)^{(n)}(\xi')(\chi_{A'}^*)^{(n)}(\lambda R\xi'). \quad \text{(A4)}$$

If $(\mathbf{F}M_\theta)(\xi')\equiv 0$ for $|\xi'|>\Xi$, and $A'>\lambda R\Xi$, then $\chi_{A'}(x')\equiv 1$ for all $x'\in[-\lambda R\Xi,\lambda R\Xi]$, and the previous expression simplifies to

$$F(\xi') = \exp(i\pi\lambda R\xi'^2)(\mathbf{F}M_\theta)(\xi'). \quad \text{(A5)}$$

As a result, we obtain the following expression for the PBI intensity:

$$(\mathbf{F}I_\theta^{\mathrm{PBI}})(\xi';R;A')/I^{\mathrm{in}} = (\mathbf{F}I_{\mathrm{FF}}^{\mathrm{PBI}})(\xi';R;A') - [\exp(-i\pi\lambda R\xi'^2)(\mathbf{F}M_\theta)(\xi') + \exp(i\pi\lambda R\xi'^2)(\mathbf{F}M_\theta)^*(-\xi')] + i[\exp(-i\pi\lambda R\xi'^2)\times(\mathbf{F}\Phi_\theta)(\xi') - \exp(i\pi\lambda R\xi'^2)(\mathbf{F}\Phi_\theta)^*(-\xi')]. \quad \text{(A6)}$$

As $\chi_{A'}$ is a real function, then both M and Φ are real and the previous expression becomes

$$(\mathbf{F}I_\theta^{\mathrm{PBI}})(\xi';R;A') = I^{\mathrm{in}}\{(\mathbf{F}I_{\mathrm{FF}}^{\mathrm{PBI}})(\xi';R;A') - 2\cos(\pi\lambda R\xi'^2)\times(\mathbf{F}M_\theta)(\xi') + 2\sin(\pi\lambda R\xi'^2)(\mathbf{F}\Phi_\theta)(\xi')\}. \quad \text{(A7)}$$

Thus, under the above conditions, the intensity in the PBI image collected with the aperture function $\chi_{A'}$ is described by Eq. (19) with μ_θ and φ_θ replaced by $(\mu_\theta\chi_{A'})$ and $(\tilde{\varphi}_\theta\chi_{A'})$, respectively.

We also assume that the smoothness of the transition of $\chi_{A'}(x')$ from 1 to 0 outside the interval $x'\in[-A',A']$ is such that the near-field condition, $|\chi_{A'}''(x')|\lambda R\ll 1$, is satisfied for all x' (alternatively, the requirement for the smoothness of the aperture edges could be relaxed if one explicitly takes into account the finite spatial resolution of the imaging system, as all image intensities would then be convolved with the PSF of the imaging system). Then we can obtain the following analog of Eq. (20) for homogeneous objects written in real space coordinates:

$$I_\theta^{\mathrm{PBI}}(x';R;A') = I^{\mathrm{in}}\{I_{\mathrm{FF}}^{\mathrm{PBI}}(x';R;A') - 2[1-\gamma\lambda R/(4\pi)\nabla^2](\mu_\theta\chi_{A'})(x')\}. \quad \text{(A8)}$$

As under the above conditions both $\chi_{A'}(x')$ and the flat-field intensity $I_{\mathrm{FF}}^{\mathrm{PBI}}(x';R;A')$ are equal to 1 within the interval $x'\in[-A,A]$, $A<A'$, and $\tilde{\varphi}_\theta\equiv\varphi_\theta$ there, then within this interval we have $I_\theta^{\mathrm{PBI}}(x';R;A')\equiv I_\theta^{\mathrm{PBI}}(x';R)$; i.e., the presence of the sufficiently wide and smooth aperture function $\chi_{A'}$ in the object plane $z=0$ does not affect the image in the plane $z=R$ inside the interval $x'\in[-A,A]$.

Similarly, for the scanning-slit intensity $I_\theta^{\mathrm{SS}}(x';R;A')$ we obtain

$$I_\theta^{\mathrm{SS}}(x';R;A') = I^{\mathrm{in}}\hat{\Lambda}_\Xi\{I_{\mathrm{FF}}^{\mathrm{PBI}}(x';R;A') - 2[1-\gamma\lambda R/(4\pi)\nabla^2](\mu_\theta\chi_{A'})(x')\}, \quad \text{(A9)}$$

where $\hat{\Lambda}_\Xi$ is the operator corresponding to the multiplication by $\Lambda_\Xi(\xi')$ in the Fourier space. It is easy to verify that $(\hat{\Lambda}_\Xi f)(x')=\Xi\int_{-\infty}^{\infty}f(x'-y)\mathrm{sinc}^2(\pi\Xi y)\mathrm{d}y$, where as usual, $\mathrm{sinc}(x)=\sin x/x$. We can represent this operator as a sum,

$$(\hat{\Lambda}_{\Xi} f)(x') = \Xi \int_{-A'}^{A'} f(y)\mathrm{sinc}^2[\pi\Xi(x'-y)]\mathrm{d}y + \Xi \int_{A'}^{\infty} f(y)\mathrm{sinc}^2[\pi\Xi(x'-y)]\mathrm{d}y + \Xi \int_{-\infty}^{-A'} f(y)\mathrm{sinc}^2[\pi\Xi(x'-y)]\mathrm{d}y. \quad \text{(A10)}$$

As for $x' \in [-A, A]$, we have

$$\left| \int_{A'}^{\infty} f(y)\mathrm{sinc}^2[\pi\Xi(x'-y)]\mathrm{d}y \right| \le \int_{A'}^{\infty} |f(y)|/[\pi\Xi(x'-y)]^2\mathrm{d}y \le |f_{\max}|/(\pi^2\Xi^2|A'-A|);$$

we can estimate the last two integrals in (A10) from above as

$$I_{\mathrm{err}} \le 2|f_{\max}|/(\pi^2\Xi|A'-A|). \quad \text{(A11)}$$

Therefore, for $x' \in [-A, A]$, we have

$$|I_\theta^{\mathrm{SS}}(x';R;A') - I_\theta^{\mathrm{SS}}(x';R)| \le 4I^{\mathrm{in}}C(\chi_{A'}, \mu_\theta)/(\pi^2\Xi|A-A'|),$$

where

$$|C(\chi_{A'}, \mu_\theta)| \le \{1 + (R/k)\max[\chi''_{A'}, (\chi'_{A'})^2]\}\{1 + \gamma\max|\mu_\theta| + \gamma(R/k)\max[|\nabla\mu_\theta|^2, |\nabla^2\mu_\theta|]\}.$$

The latter term is less than $4+2\max|\varphi_\theta|$ owing to the assumptions made about the weakness of absorption and about the near-field conditions for both $\chi_{A'}$ and μ_θ. Hence we obtain

$$|I_\theta^{\mathrm{SS}}(x';R;A') - I_\theta^{\mathrm{SS}}(x';R)| \le (16 + 8\max|\varphi_\theta|)I^{\mathrm{in}}/(\pi^2\Xi|A-A'|). \quad \text{(A12)}$$

The last inequality, in combination with Eq. (A8), shows that for sufficiently large A', the contrast function $K_\theta^{\mathrm{SS}}(x',y;R;A') \equiv [I_\theta^{\mathrm{PBI}}(x',y;R;A') - I_\theta^{\mathrm{SS}}(x',y;R;A')]/I^{\mathrm{in}}$ within the interval $x' \in [-A, A]$ can be made arbitrarily close to the function $K_\theta^{\mathrm{SS}}(x',y;R) \equiv [I_\theta^{\mathrm{PBI}}(x',y;R) - I_\theta^{\mathrm{SS}}(x',y;R)]/I^{\mathrm{in}}$. Since we have already shown that the knowledge of the contrast function $K_\theta^{\mathrm{SS}}(x',y;R)$ within the interval $x' \in [-A, A]$ is sufficient for the CT reconstruction of the absorptive index or its derivatives within the disk $x^2+z^2 \le A^2$ [in accordance with Eqs. (24)–(26)], this completes the proof that the local CT with the limiting aperture in the object plane is also possible, provided that the aperture is sufficiently wider [as required by Eq. (A12)] than the projection of the ROI.

Note that although the error estimate in Eq. (A12) can seemingly be decreased by increasing the value of the cutoff frequency Ξ, the resultant contrast function is multiplied by the factor $d/R = \lambda\Xi$ in the process of reconstruction of the absorptive index in accordance with Eqs. (24)–(26). Therefore, an increase in the cutoff frequency would lead to more unstable reconstruction. This is consistent with the physics of the proposed reconstruction scheme. Indeed, an increase in Ξ means an effective broadening of the scanning slit, which diminishes the difference between the scanning-slit intensity and the PBI intensity collected without the scanning slit, i.e., it decreases the contrast function $K_\theta^{\mathrm{SS}}(x',y;R) \equiv [I_\theta^{\mathrm{PBI}}(x',y;R) - I_\theta^{\mathrm{SS}}(x',y;R)]/I^{\mathrm{in}}$, making the reconstruction susceptible to noise.

REFERENCES

1. G. T. Herman, *Image Reconstruction from Projections. The Fundamentals of Computerized Tomography* (Academic, 1980).
2. M. Born and E. Wolf, *Principles of Optics*, 7th (expanded) ed. (Cambridge U. Press, 1999).
3. F. Natterer, *The Mathematics of Computerized Tomography* (Wiley, 1986).
4. E. Wolf, "Three-dimensional structure determination of semi-transparent objects from holographic data," Opt. Commun. **1**, 153–156 (1969).
5. G. Gbur and W. Wolf, "Diffraction tomography without phase information," Opt. Lett. **27**, 1890–1892 (2002).
6. M. A. Anastasio and D. Shi, "On the relationship between intensity diffraction tomography and phase-contrast tomography," Proc. SPIE **5535**, 361–368 (2004).
7. A. Momose, T. Takeda, and Y. Itai, "X-ray computed tomography for observing biological specimens and organic materials," Rev. Sci. Instrum. **66**, 1434–1436 (1995).
8. U. Bonse and F. Busch, "X-ray computed microtomography (μCT) using synchrotron radiation (SR)," Prog. Biophys. Mol. Biol. **65**, 133–169 (1996).
9. C. Raven, A. Snigirev, I. Snigireva, P. Spanne, A. Souvorov, and V. Kohn, "Phase-contrast microtomography with coherent high-energy synchrotron x-rays," Appl. Phys. Lett. **69**, 1826–1828 (1996).
10. P. Cloetens, M. Pateyron-Salome, J. Y. Buffiere, G. Peix, J. Baruchel, F. Peyrin, and M. Schlenker, "Observation of microstructure and damage in materials by phase sensitive radiography and tomography," J. Appl. Phys. **81**, 5878–5886 (1997).
11. A. V. Bronnikov, "Reconstruction formulas in phase-contrast tomography," Opt. Commun. **171**, 239–242 (1999).
12. S. C. Mayo, T. J. Davis, T. E. Gureyev, P. R. Miller, D. Paganin, A. Pogany, A. W. Stevenson, and S. W. Wilkins, "X-ray phase-contrast microscopy and microtomography," Opt. Express **11**, 2289–2302 (2003).
13. G. Schmahl and D. Rudolf, "Proposal for a phase contrast x-ray microscope" in *X-ray Microscopy*, P. Cheng and G. J. Jan, eds., (Springer-Verlag, 1987), pp. 231–238.
14. A. Snigirev, V. Kohn, I. Snigireva, and B. Lengeler, "A compound refractive lens for focusing high-energy x-rays," Nature **384**, 49–51 (1996).
15. F. A. Dilmanian, Z. Zhong, B. Ren, X. Y. Wu, L. D. Chapman, I. Orion, and W. C. Thomlinson, "Computed tomography of x-ray index of refraction using the diffraction enhanced imaging method," Phys. Med. Biol. **45**, 933–946 (2000).
16. K. M. Pavlov, C. M. Kewish, J. R. Davis, and M. J. Morgan, "A variant on the geometrical optics approximation in diffraction enhanced tomography," J. Phys. D **34**, A168–A172 (2001).
17. I. Koyama, A. Momose, J. Wu, T. T. Lwin, and T. Takeda, "Biological imaging by x-ray phase tomography using diffraction enhanced imaging," Jpn. J. Appl. Phys. **44**, 8219–8221 (2005).
18. A. G. Ramm and A. I. Katsevich, *The Radon Transform and Local Tomography* (CRC Press, 1996).
19. M. A. Anastasio, D. Shi, F. De Carlo, and X. Pan, "Analytic image reconstruction in local phase-contrast tomography," Phys. Med. Biol. **49**, 121–144 (2004).
20. F. Noo, R. Clackdoyle, and J. D. Pack, "A two-step Hilbert transform method for 2D image reconstruction," Phys. Med. Biol. **49**, 3903–3923 (2004).
21. J.-P. Guigay, "Fourier transform analysis of Fresnel diffraction patterns and in-line holograms," Optik (Stuttgart) **49**, 121–125 (1977).

22. T. E. Gureyev, Ya. I. Nesterets, D. M. Paganin, A. Pogany, and S. W. Wilkins, "Linear algorithms for phase retrieval in the Fresnel region. 2. Partially coherent illumination," Opt. Commun. **259**, 569–580 (2006).
23. Ya. I. Nesterets, T. E. Gureyev, and S. W. Wilkins, "Polychromaticity in the combined propagation-based/analyser-based phase-contrast imaging," J. Phys. D **38**, 4259–4271 (2005).
24. T. E. Gureyev, G. R. Myers, Ya. I. Nesterets, D. M. Paganin, K. M. Pavlov, S. C. Mayo, and S. W. Wilkins, "Stability and locality of amplitude and phase contrast tomographies," Proc. SPIE **6318**, 63180V (2006).
25. Ya. I. Nesterets, T. E. Gureyev, and S. W. Wilkins, "General reconstruction formulas for analyzer-based computed tomography," Appl. Phys. Lett. **89**, 264103 (2006).
26. Ya. I. Nesterets, T. E. Gureyev, and S. W. Wilkins, "Local tomography with a scanning slit aperture, in preparation." (Tim.Gureyev@csiro.au)
27. D. Paganin, S. C. Mayo, T. E. Gureyev, P. R. Miller, and S. W. Wilkins, "Simultaneous phase and amplitude extraction from a single defocused image of a homogeneous object," J. Microsc. **206**, 33–40 (2002).
28. X. Wu and H. Liu, "A reconstruction formula for soft tissue x-ray phase tomography," J. X-Ray Sci. Technol. **12**, 273–279 (2004).
29. T. E. Gureyev, A. W. Stevenson, Ya. I. Nesterets, and S. W. Wilkins, "Image deblurring by means of defocus," Opt. Commun. **240**, 81–88 (2004).
30. T. E. Gureyev, A. W. Stevenson, D. M. Paganin, T. Weitkamp, A. Snigirev, I. Snigireva, and S. W. Wilkins, "Quantitative analysis of two-component samples using in-line hard x-ray images," J. Synchrotron Radiat. **9**, 148–153 (2002).